

We are IntechOpen, the world's leading publisher of Open Access books Built by scientists, for scientists

6,900

Open access books available

185,000

International authors and editors

200M

Downloads

Our authors are among the

154

Countries delivered to

TOP 1%

most cited scientists

12.2%

Contributors from top 500 universities



WEB OF SCIENCE™

Selection of our books indexed in the Book Citation Index
in Web of Science™ Core Collection (BKCI)

Interested in publishing with us?
Contact book.department@intechopen.com

Numbers displayed above are based on latest data collected.
For more information visit www.intechopen.com



Nanoscale Plasmon Sources: Physical Principles and Novel Structures

Hamed Ghodsi and Hassan Kaatuzian

Abstract

Started by M. Stockman with his proposed idea of a nanoscale quantum generator of plasmons that he called surface plasmon amplification by stimulated emission of radiation (SPASER) in 2002, during the last two decades various devices have been proposed, fabricated, and tested for SPASERs or plasmonic nanolasers which have almost the same meaning. Despite all these efforts, there are still serious barriers in front of these devices to be an ideal nanoscale coherent source of surface plasmons. The main challenges are the difficulty of fabrication, over-heating, low output powers, high loss rates, lack of integration capability with commercial fabrication processes, inefficient performance in room temperature, and so on. In this chapter, governing principles of nanolaser operation are discussed. Important parameters, limitations, and design challenges are explained, and some of the proposed or fabricated structures are presented and their merits and demerits are expressed. Eventually, several novel structures resulting from our works are introduced, and their performances are compared to the state-of-the-art structures.

Keywords: nanoscale plasmon source, SPASER, plasmonic nanolaser, nanoplasmonics, stimulated emission

1. Introduction

Theoretical postulation [1] and realization of laser [2] in the twentieth century changed both science and technology forever. Potential applications of lasers later have enormously expanded by the invention of the semiconductor diode laser in 1962 which brought them into the commercial market and in almost every device we know [3]. In the 1990s by the introduction of vertical-cavity surface-emitting laser (VCSEL) diodes, semiconductor lasers have pushed to their size limits [4]. The size of a dielectric cavity laser cannot be smaller than $\lambda/2$ in each dimension, and this limitation is known as the diffraction limit. With this in mind, modern VCSEL sizes are limited to a few microns [5]. On the other hand from the beginning of the millennia due to the rapid development of fabrication methods and tools [6], submicron manipulation of light using plasmonic devices has got lots of attention [7–10]. Plasmonic structures using metal/insulator interfaces broke the size limitation of the photonic devices and paved the way for integrating electronics, photonics, and optoelectronics on a single monolithic chip [11].

In order to bring benefits of the plasmonics into the field of laser research and fabrication, M. Stockman proposed the idea of a nanoscale quantum generator

called surface plasmon amplification by stimulated emission of radiation (SPASER) in 2002 [12]. This device utilizes a plasmonic feedback mechanism in a gain medium for exciting stimulated emission in local plasmon modes of metallic nanoparticles. In the next two decades, various mechanisms and devices have been proposed and fabricated for the realization of a nanoscale coherent plasmon source or plasmonic nanolaser [13]. These devices can be categorized in nanoparticles [12], waveguide-based nanolasers [15], nanowires [16], nanoresonators [17], nanopatches [18], nanodisks [19], plasmonic crystals [20], and so on. Although these devices have shown significant potentials, there are still serious problems with the nanoscale coherent sources of surface plasmons. For instance, the difficulty of fabrication, over-heating, low output powers, high loss rates, lack of integration capability with commercial fabrication processes like CMOS, inefficient performance in room temperature, and so on can be noted [12, 13].

In this chapter and in Section 2, we start with basic principles of nanoplasmonics like the definition of surface plasmon polariton (SPP) modes in classical and quantum mechanical pictures, different sources of plasmon loss, and specific properties of plasmons focusing on special characteristics of plasmons in metallic nanoresonators. Then, the interaction of plasmons with carriers in a cavity will be briefly discussed according to plasmonic cavity quantum electrodynamics. In Section 3, three different methods for analyzing plasmonic nanolasers are discussed, and in Section 4 several previously introduced nanolaser structures are briefly reviewed. In Section 5, the proposed nanolaser structures by the authors are introduced, and this chapter will be concluded in Section 6.

2. Nanoplasmonics and quantum treatment of plasmons

The modern era of plasmonic began with the investigation of wood anomalies in the early twentieth century [21]. Later in 1957 Ritchie published a paper on plasma loss due to the electrons at the interface of a thin metal film [11]. In the next few years, theoretical works on collective oscillations of electrons at the surface of metals led to the introduction of plasmons as the quasiparticle corresponding to these oscillations [11]. However, applications of plasmons as a tool for nanoscale manipulation of light has gained significant attention with the paper by H. Atwater in 2007 named “Promise of plasmonics” [21]. In the past two decades, plasmonics has been developed both in theoretical and experimental aspects, and many different devices like switches [22], detectors [23], routers [24], amplifiers [25], and sources [17] have been introduced.

2.1 Basic principles

In order to find an appropriate model for surface plasma waves at the surface of a metal, we should deal with a charge density wave in an infinite electron gas which is often modeled by hydrodynamic equations [11]. An electromagnetic wave propagating in a material polarizes it and results in a mechanical excitation in electric charges and their movement. Therefore, oscillations in the electric field and mechanical oscillations are coupled. This coupled oscillation is called polariton. In case of metals, the electromagnetic field causes a longitudinal wave of charge density, and the coupled oscillations are known as plasmon polariton waves [11].

According to **Figure 1** at the interface of metal with a dielectric interaction of an electromagnetic field with the surface electrons, a specific type of plasmon polariton waves called surface plasmon polaritons or SPP modes results. Although

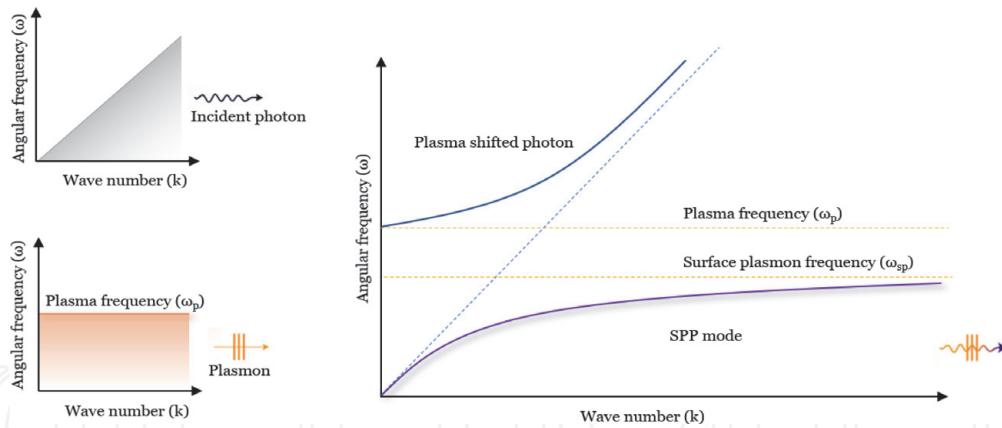


Figure 1. Interaction of an electromagnetic field with surface plasma waves and excitation of surface plasmon polariton waves.

there are different types of plasmons like bulk plasmons and local surface plasmons (LSPs), SPP and LSP modes have significant roles in many plasmonic devices.

There are several models for plasmons, and we are going to briefly overview them here. The most well-known and simple model is Drude's model which describes the metal as a free electron gas system and models the system using the classical spring-mass model with the external force exerted from the incident field "E" equals to "-qE" acting on the system. We are not going to derive the equations here and only use the final result as shown in Eq. (1) which can be derived as mentioned in many related references like [22]:

$$\epsilon_r(\omega) = 1 - \frac{\omega_p^2}{\omega^2 + i\gamma(\omega)\omega}, \quad \omega_p^2 = \frac{ne^2}{\epsilon_0 m}, \quad \gamma = \frac{1}{\tau} \quad (1)$$

where "n" is number of electrons in the unit volume of the metal, "e" is the electron charge, "m" is the electron mass, " ϵ_0 " is permittivity of vacuum, " ω_p " is the plasma frequency of the metal, " γ " is the total loss, and " τ " is the effective lifetime of the electrons associated with all of the decay processes.

According to Eq. (1), permittivity of a metal $\epsilon_r(\omega)$ can be used in solving Helmholtz equations and finding the behavior of electromagnetic waves propagating at the metal/dielectric interface which are also known as SPP waves. However, Drude's model suffers from several shortcomings which leads to considerable errors especially near the plasma frequency of the metal. This is because in Drude's model, the effect of electrons in other energy bands (not just free electrons) is not included, and nonlocal effects are also not included [26]. To overcome these problems, Drude-Lorentz's model is introduced for the first problem which can be written in general multi-oscillator form as Eq. (2) and Landau damping correction according to Eq. (3) for the second problem. We are not going to further discuss these models either, and you can find details in [11, 26].

$$\epsilon_{\text{Drude-Lorentz}}(\omega) = 1 - \frac{f_0 \omega_{p,0}^2}{\omega^2 + i\gamma_0 \omega} + \sum_{j=1}^{j_{\max}} \frac{f_j \omega_{p,j}^2}{\omega_j^2 - \omega^2 - i\gamma_j \omega} \quad (2)$$

where the first sentence corresponds to Drude's model; " f_j " is the power of the j 'th oscillator; and " $\omega_{p,j}$ ", " ω_j ", and " γ_j " are plasma frequency, resonant frequency, and loss coefficient of the j 'th oscillator, respectively.

$$\epsilon_r(\omega) = 1 - \frac{\omega_p^2}{\omega^2 + i\gamma(\omega)\omega - \beta k^2}, \quad \omega_p^2 = \frac{ne^2}{\epsilon_0 m}, \quad \gamma = \frac{1}{\tau} \quad (3)$$

where “ β ” is the Landau nonlocal parameter which becomes important for large values of wavenumber.

More precise treatment of surface plasmons can be done using the hydrodynamic model which includes solving Bloch equations, i.e., continuity, and Bernoulli and Poisson’s equations simultaneously. According to Eqs. (4–6), one can describe collective oscillations of electrons in an arbitrary system using electron density (n) and hydrodynamic velocity ($v(r, t) = -\nabla\psi(r, t)$) [23].

$$\frac{d}{dt}n(r, t) = \nabla n(r, t) = \nabla \cdot [n(r, t)\nabla\psi(r, t)] \quad (4)$$

$$\frac{d}{dt}\psi(r, t) = \frac{1}{2}|\nabla\psi(r, t)|^2 + \frac{\delta G[n]}{\delta n} + \phi(r, t) \quad (5)$$

$$G[n] = \frac{3}{10}(3\pi^2)^{\frac{2}{3}}[n(r, t)]^{\frac{5}{3}}$$

$$\nabla^2\phi(r, t) = 4\pi n(r, t) \quad (6)$$

In the general form, Bloch equations are nonlinear and quite difficult to solve. However, using the perturbation theory, one can find linearized equations of Eq. (7) which helped Ritchie and his team to find plasmon dispersion equation in Eq. (8) for the first time [23].

$$\begin{aligned} n(r, t) &= n_0(r) + n_1(r, t) + \dots \\ \psi(r, t) &= 0 + \psi_1(r, t) + \dots \\ \begin{cases} \frac{d}{dt}n_1(r, t) = \nabla \cdot [n_0(r)\nabla\psi_1(r, t)] \\ \frac{d}{dt}\psi_1(r, t) = [\beta(r)]^2 \frac{n_1(r, t)}{n_0(r)} + \phi(r, t) \\ \nabla^2\phi_1(r, t) = 4\pi n_1(r, t) \end{cases} \end{aligned} \quad (7)$$

$$\begin{aligned} \omega^2 &= \frac{1}{2} \left[\omega_p^2 + \beta^2 k^2 + \beta k \sqrt{2\omega_p^2 + \beta^2 k^2} \right] \\ \frac{\beta k}{\omega_p} \ll 1 &\rightarrow \omega = \frac{\omega_p}{\sqrt{2}} + \frac{\beta k}{2} \end{aligned} \quad (8)$$

The most accurate model for dealing with surface plasmons in atomic scales is solving Schrodinger’s equation and calculating dynamical structure factor in Eq. (9) which is related to the oscillations of particle density in a many-particle system [23]:

$$S(r, r'; \omega) = \sum_n \delta\hat{\rho}_{0n}(r_1)\delta\hat{\rho}_{n0}(r_2)\delta(\omega - E_n + E_0) \quad (9)$$

where the first two terms are elements of the operator “ $\rho(r)-n_0(r)$ ” relating the ground state “ ψ_0 ” with energy “ E_0 ” and “ δ ” is the Dirac function, “ $n_0(r)$ ” represents ground state density of particles, and “ $\rho(r)$ ” is the particle density operator.

Using this model one can precisely calculate electron density profile in a many-electron system like a metal. However, solving the required equations is not easy, and most often approximations like random phase approximation or time-dependent density functional theory is used [23].

2.2 Specific properties of surface plasmons

Various applications of plasmonic technology in development of nanoscale devices and systems are all based on the same fundamental properties of plasmons. These specific properties include field confinement, enhancement of local density of optical states, and ultrawide bandwidth and fast response [11].

Confinement of electromagnetic fields in scales much smaller than the wavelength is the most crucial property of surface plasmon modes and can be defined in both parallel and orthogonal planes. Due to the high rate of loss, propagation length of the surface plasma waves in any direction is inversely related to the imaginary part of the wavenumber “ $1/\text{Im}(k_{sp})$.” This length for good plasmonic metals like gold and silver is limited to a few microns and is considered as the upper limit of confinement [11]. The lower limit of confinement is exerted by Fourier transform properties with considering a monochromatic field with frequency “ ω ” and wavenumber “ $k = \omega/c$ ” in the vacuum with far from any surface. It can be concluded that in the “ x ” direction “ $\Delta x \Delta \alpha \geq 2\pi$ ” in which α is the x component of the wavenumber. Therefore, the lower limit of field confinement is “ $2\pi/\alpha_{\max} = \lambda$ ” which is also known as the diffraction limit. However, for surface plasmons, the wavenumber according to the dispersion relation (see **Figure 1**) can be much higher than “ ω/c ” which implies that surface plasmon modes can be confined in extremely tiny dimensions (much smaller than the wavelength) [11].

Enhancement of local density of optical states (LDOS) for surface plasmons can be investigated both near the metal surface and in a metallic nanoresonator. In a metallic nanoresonator, this effect which is also known as Purcell effect or enhancement of spontaneous emission is the vital property of plasmonic nanolasers. Purcell factor (F_p) is defined by the ratio of decay rate due to the spontaneous emission in a cavity over the decay rate in the free space. It can be calculated by Fermi’s golden rule in a two-level atomic system and expressed by Eq. (10) [24].

$$\frac{\Gamma_{cav}}{n_1 \Gamma_0} = \frac{3}{4\pi^2} \left(\frac{\lambda_{em}}{n_1} \right)^3 \frac{Q}{V_{eff}} \frac{|\hat{u} \cdot \vec{f}(\vec{r})|^2}{1 + 4Q^2 \left(\frac{\omega_{em} - \omega_c}{\omega_c} \right)^2} = F_p \frac{|\hat{u} \cdot \vec{f}(\vec{r})|^2}{1 + 4Q^2 \left(\frac{\omega_{em} - \omega_c}{\omega_c} \right)^2} \quad (10)$$

$$F_p = \frac{3}{4\pi^2} \left(\frac{\lambda_{em}}{n_1} \right)^3 \frac{Q}{V_{eff}}$$

In which “ Γ_{cav} ” is the decay rate in the cavity, “ Γ_0 ” is the decay rate in the free space, “ n_1 ” is the refractive index of the propagation medium, “ λ_{em} ” and “ ω_{em} ” are the emission wavelength of the medium, “ ω_c ” is the cavity resonance frequency, “ Q ” is the quality factor of the cavity, “ V_{eff} ” is the effective mode volume of the propagating mode in the cavity, and the dot product of the nominator corresponds to the mismatch between directions of transition dipole and the field.

In a dielectric microcavity despite the large quality factor, large mode volume results in infinitesimal Purcell factors, but nanoscale metallic resonators (the building block of a plasmonic nanolaser) provide a very small equivalent mode volume expressed by Eq. (11) which results in a large Purcell factor which is crucial for the nanolaser operation. Moreover, since the emission rate is proportional to the LDOS, the higher Purcell factor means the higher local density of optical states [24].

$$V_{eff} = \frac{\int \epsilon(\vec{r}) |\vec{E}(\vec{r})|^2 dr}{\text{Max} \left[\epsilon(\vec{r}) |\vec{E}(\vec{r})|^2 \right]} \quad (11)$$

where “ $\varepsilon(r)$ ” is the permittivity as a function of position inside the resonator volume in which the integral is calculated and “ $E(r)$ ” is the electrical field related to the propagating mode. However, this condition for a plasmonic nanocavity may not be satisfied. Therefore, the electromagnetic energy density of a dispersive and dissipative medium should be used in Eq. (11). A dispersive lossless medium like the dielectric side of the interface (12) can provide a good estimation and a lossy medium like the metal side of the interface (13) should be used [25].

$$\langle u \rangle = \frac{1}{2} \varepsilon_0 |E(\vec{r})|^2 \left(\varepsilon'_r(r, \omega) + \omega \frac{\partial \varepsilon'_r(r, \omega)}{\partial \omega} \right) \quad (12)$$

where “ $\varepsilon'(r)$ ” is the real part of the permittivity.

$$\langle u \rangle = \frac{1}{4} \varepsilon_0 |E(\vec{r})|^2 \left(\varepsilon'_r(r, \omega) + \frac{2\varepsilon''_r(r, \omega)\omega}{\gamma} \right) \quad (13)$$

where “ $\varepsilon''(r)$ ” is the real part of the permittivity and “ γ ” is the loss rate introduced in Drude’s model.

The third specific property of surface plasmons is their ultrawide bandwidths and fast response. In plasmonic nanoresonators due to considerable loss levels, quality factor is limited and in many cases between 10 and 100. Low-quality factor despite its negative effect on the Purcell factor provides an ultrawide bandwidth of several terahertz. This wide bandwidth resulting in fast time response has applications in generating femtosecond pulses in nanoscale dimensions and ultra-wideband nanoantennas [11].

2.3 Plasmon loss mechanisms

Inherent lossy nature of plasmon propagations requires more attention to the loss mechanisms both for using the loss as a beneficial application like biomarkers and biosensors [13] and minimizing its unwanted effects like plasmonic nanolasers.

Surface plasmons decay because of several elastic or inelastic loss channels, for instance, scattering because of other electrons, phonons, or crystal defects and so on. We will categorize them into three groups. The first is bulk decay rate or (γ_b) which can be expressed by Eq. (14) [26].

$$\gamma_b = \gamma_{e-e} + \gamma_{e-phonon} + \gamma_{e-defect} + \dots \quad (14)$$

which the first term is due to electron-electron scattering as can be derived by Eq. (15) and the second term is due to electron-phonon scattering mechanism. Furthermore, the third term is the electron-defect decay rate. It should be noticed that for metals in the room temperature, electron-phonon decay rate is about 10^{14} Hz and increases with the temperature. But, the other two factors remain constant with the temperature and exist even in the absolute zero [26].

$$\gamma_{e-e} \approx 10^{15} \cdot \left(\frac{\hbar\omega}{E_F} \right)^2 \text{ Hz} \quad (15)$$

As can be seen from Eq. (15), the electron-electron scattering has a direct relation with the frequency and in the visible frequencies is in the same order of magnitude as the first term [26].

In the plasmonic structures with dimensions about few nanometers, i.e., shorter than the mean free path of electrons, the second type of decay should be considered.

Surface scattering due to roughness of the surface (γ_{sc}) is inversely related to the mean free path due to surface roughness (a) and directly proportional to the Fermi velocity of electrons [26]. Fermi velocity is the maximum velocity an electron can achieve due to Fermi-Dirac distribution. For instant, for gold Fermi velocity is about 2.5×10^6 m/s.

The third type of losses in plasmonic devices is because of a process called Landau's damping [26]. Landau damping arises from the electrons oscillating with the velocity equal to the phase velocity of the surface plasmon mode. During acceleration, these electrons absorb energy from the plasmon mode. In other words, a quanta (plasmon) of the surface plasma wave is annihilated, and an electron-hole pair is generated in this procedure. Simply put, Landau damping is the plasmon-electron interaction mechanism. Landau damping rate (γ_L) which is significant for the large wavenumber values (see **Figure 2**) can be estimated by Eq. (16) [26].

$$\gamma_L \approx \omega_p \cdot \left(\frac{k_D}{k}\right)^3 \cdot \exp\left(\frac{-k_D^2}{2k^2}\right), k_D = \frac{\omega_p}{v_F} \tag{16}$$

2.4 Surface plasmons in quantum mechanical picture

Plasmonic nanolasers are considered to be quantum nanogenerators of surface plasmons. Similar to lasers, these devices also operate based on both particle and wave properties of the electromagnetic waves. Therefore, finding a valid quantization approach for surface plasmon modes is necessary for explaining operation principles of the nanolasers.

The first attempts for finding a quantized description of plasmons are done by Bohm and Pines in the 1950s, and their works lead to the Pines model. In the Pines model, metal is considered to be a free electron gas material and electrons share long-range correlations in their positions in the form of collective oscillations in the whole system [27]. Pines model describes a quantized model of these collective

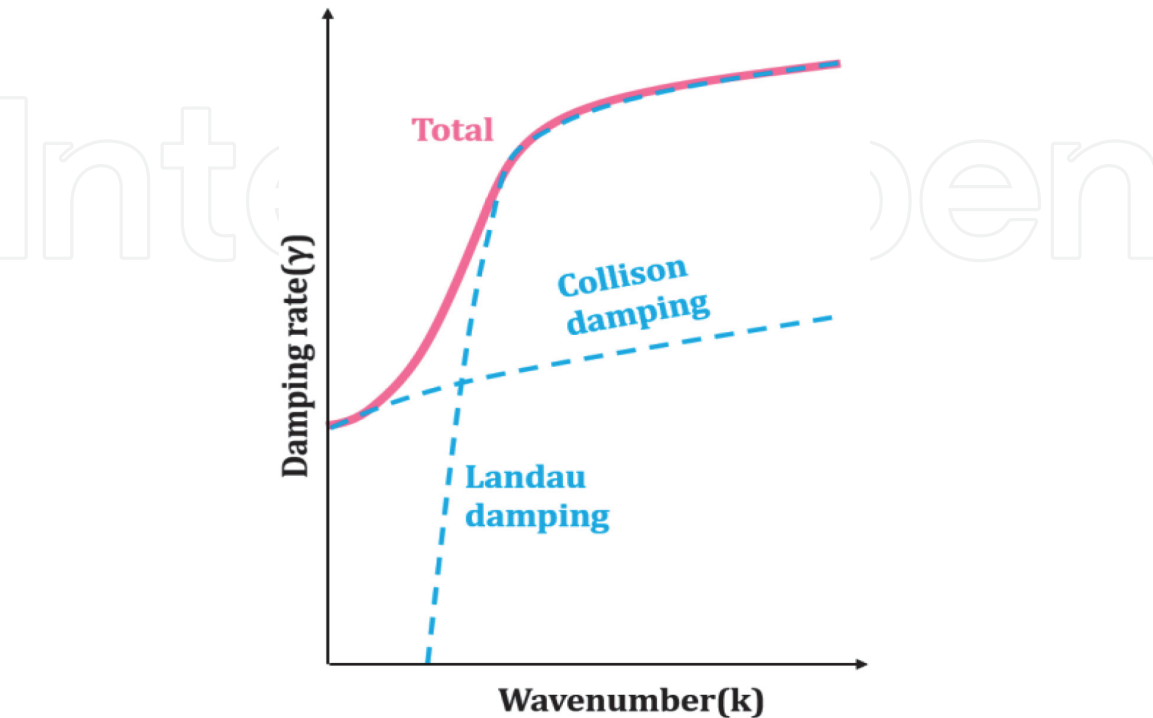


Figure 2.
Landau damping effect on the total damping rate [26].

oscillations which have both wave and particle properties, and the corresponding quanta (plasmon) is a boson [27].

Polariton is a joint state of light and matter introduced by Hopfield for providing a quantum model for the polarization field describing the response of matter to light [30]. Based on Hopfield's model, Ritchie and Elson proposed the first quantized description of surface plasma waves called Surface Plasmon Polariton or SPP. However, Hopfield's model did not consider the scattering and loss in the metal and effects of valence electrons and later Huttner and Barnett propose a model based on the Hopfield model including dispersion and loss, and recently a macroscopic quantization model based on Green's functions has also been published [27].

3. Physical models for analyzing plasmonic nanolasers

In order to analyze a plasmonic nanolaser, we need theoretical tools for describing the carrier-plasmon dynamics in the cavity. In this section, several models are discussed with different precision, but every method has its own limitations and should be used for a specific category of devices or a certain purpose.

3.1 Plasmon cavity quantum electrodynamics (PCQED)

Interaction of electron-hole pairs and plasmons in a nanocavity is the fundamental mechanism in any plasmonic nanolaser. As an example of this interaction, energy transfer diagram in a quantum well based nanolaser is illustrated in **Figure 3**.

This interaction should be treated similar to light-matter interaction in a laser cavity by the cavity quantum electrodynamics (CQED). However, in a plasmonic nanocavity due to Purcell enhancement of spontaneous emission and nanoscale dimensions and considerable loss and dispersion, there should be considerable differences that lead to a new cavity electrodynamic model for plasmonic cavities or PCQED [14].

The key difference between CQED and PCQED is in the method of controlling the interaction of electromagnetic fields with the medium. One of the most fundamental differences between them is the enhancement of spontaneous emission rate in a plasmonic cavity by the Purcell factor. The physical structure of the cavity affects the spectral characteristics of the plasmonic mode oscillations and results in a difference in the local density of optical states and the Purcell factor based on the designer's will. In other words, CQED controls interaction dynamics by their relationship with the quality factor of the resonator, while in PCQED dynamic of interactions is controlled by the Purcell factor. In dielectric microcavities, the quality factor is very high (even 10^{10}), while modal volume is limited to the refraction limit (few microns in each dimension), and Purcell enhancement does not occur. On the other hand, for plasmonic nanocavities because of intense mode confinement, equivalent mode volume is far smaller than the diffraction limit and results in considerable Purcell factor and density of state manipulation [14].

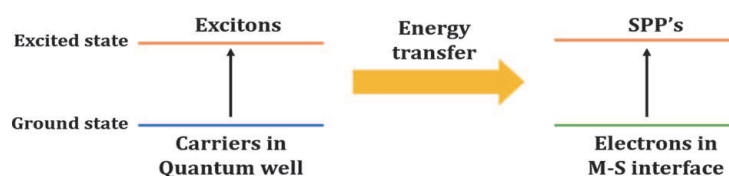


Figure 3.
Energy transfer diagram of a quantum-well based nanolaser.

Moreover, in PCQED loss and dispersion are critical factors and are necessary for correct modeling. Finding precise quantum mechanical models for these phenomena in plasmonic nanocavities still needs more research. However, we can use the photon/plasmon analogy and developed methods and tools of the photons like the density of state matrix and decay channels for estimating quantum mechanical behavior of plasmonic nanocavities [14].

3.2 Quantum mechanical atomic-scale model

Modeling phenomena like quantum fluctuations, spectral narrowing, coherency, threshold behavior, and precise dynamic analysis of plasmon nanolasers need an atomic-scale quantum mechanical model. However, in order to find closed-form equations, several simplifications are necessary, and thus this model just provides a theoretical tool for investigating fundamental properties of plasmonic nanolasers.

To do so, consider an N-atom system in a low-quality factor nanocavity in which the decay rate of the cavity (κ) is the fastest decay rate of this system. This condition is called the “bad cavity assumption” [28]. Therefore, resonator mode can be adiabatically eliminated, and the system state is totally determined by “N” active atoms. Considering two energy levels for each atom which are coupled to a cavity with resonance frequency (ω) and plasmon lifetime ($1/2\kappa$), one can describe the interactions between the atoms and field by Tavis-Cumming Hamiltonian of Eq. (17) [28].

$$H_{AF} = i\hbar g(a^\dagger J_- - a J_+) \quad (17)$$

In which “ g ” is the coupling factor which is identical for all of the atoms, “ a ” and “ a^\dagger ” are annihilation and creation operators of plasmons, respectively, and “ J_α ” is the operator of collective atomic oscillations in the “ α ” direction and can be defined by Eq. (18) in which “ σ_{jx} ” and “ σ_{jy} ” are Pauli matrices [28].

$$J_\alpha = \sum_{j=1}^N \sigma_{j\alpha}, \quad \alpha = \{x, y, z\}, \quad \sigma_{j\pm} = \frac{\sigma_{jx} \pm i\sigma_{jy}}{2} \quad (18)$$

Using atomic density operator “ ρ ” in a quantum system with state vector “ ψ ” and by considering the Hamiltonian of Eq. (17), Schrodinger’s equation leads us to the dynamic equation of Eq. (19) in which “ γ_\uparrow ” is the pumping rate and “ γ_\downarrow ” is the spontaneous emission rate and “ γ_p ” is the dephasing rate of oscillating atoms [28]. The last term describes interaction of active atoms through the cavity mode [28].

$$\begin{aligned} \dot{\rho} = & -i\frac{1}{2}\omega[J_z, \rho] + \frac{\gamma_\uparrow}{2} \left(\sum_{j=1}^N 2\sigma_{j+}\rho\sigma_{j-} + \frac{1}{2}J_z\rho + \frac{1}{2}\rho J_z - N\rho \right) \\ & + \frac{\gamma_\downarrow}{2} \left(\sum_{j=1}^N 2\sigma_{j-}\rho\sigma_{j+} - \frac{1}{2}J_z\rho - \frac{1}{2}\rho J_z - N\rho \right) + \frac{\gamma_p}{2} \left(\sum_{j=1}^N 2\sigma_{jz}\rho\sigma_{jz} - N\rho \right) + \frac{g^2}{\kappa} (2J_- \rho) \end{aligned} \quad (19)$$

After several mathematic manipulations on Eq. (19) and by defining “ $X_N(\xi, \xi^*, \eta) = \text{tr}(\rho e^{i\xi^* J_+} e^{i\eta J_z} e^{i\xi J_-})$ ” and its Fourier transform “ $\tilde{P}(v, v^*, m)$ ” as the atomic polarization operator, we can conclude Eq. (20) as a closed-form dynamic equation describing the system by collective atomic operators [28].

$$\begin{aligned}
 \frac{\partial \tilde{P}}{\partial t} &= L \left(v, v^*, m, \frac{\partial}{\partial v}, \frac{\partial}{\partial v^*}, \frac{\partial}{\partial m} \right) \tilde{P} \\
 L &= \frac{\gamma_{\uparrow}}{2} \left[\left(e^{-2\frac{\partial}{\partial m}} - 1 \right) (N - m) + \frac{\partial^4}{\partial v^2 \partial v^{*2}} e^{2\frac{\partial}{\partial m}} (N + m) + 2N \frac{\partial^2}{\partial v \partial v^*} \right] + \\
 &\quad + \frac{\gamma_{\uparrow}}{2} \left(2e^{-2\frac{\partial}{\partial m}} - 1 + \frac{2\partial^2}{\partial v \partial v^*} \right) \left(\frac{\partial}{\partial v} v + \frac{\partial}{\partial v^*} v^* \right) + \\
 &\quad + \frac{\gamma_{\downarrow}}{2} \left[\left(e^{2\frac{\partial}{\partial m}} - 1 \right) (N + m) + \frac{\partial}{\partial v} v + \frac{\partial}{\partial v^*} v^* \right] + \\
 &\quad + \gamma_p \left[\frac{\partial}{\partial v} v + \frac{\partial}{\partial v^*} v^* + \frac{\partial^2}{\partial v \partial v^*} e^{2\frac{\partial}{\partial m}} (N + m) \right] + i\omega \left[\frac{\partial}{\partial v} v + \frac{\partial}{\partial v^*} v^* \right] + \\
 &\quad + \frac{g^2}{\kappa} \left[2 \left(1 - e^{-2\frac{\partial}{\partial m}} \right) v v^* - \left(\frac{\partial}{\partial v} v m + \frac{\partial}{\partial v^*} v^* m \right) + \frac{\partial^2}{\partial v^2} v^2 + \frac{\partial^2}{\partial v^{*2}} v^{*2} \right]
 \end{aligned} \tag{20}$$

It should be noticed that Eq. (20) has not an analytical solution in this form and should be linearized or be solved numerically. In order to find a more familiar form of the dynamic rate equations, we should use linearization. By defining plasmon mode using dimensionless polarization “ σ ” and number of carriers by normalized population inversion “ n ,” one can write Eq. (21) for a plasmonic nanolaser with N active atoms and the mentioned assumptions [28]:

$$\begin{aligned}
 \frac{d\left(\frac{\sigma}{n_s}\right)}{\Gamma dt} &= - \left(1 - \wp \frac{n}{n_s} \right) \frac{\sigma}{n_s}, \sigma = \text{tr}[\rho J_- e^{i\omega t}] / N, n = \text{tr}[\rho J_z] / N \\
 \frac{d\left(\frac{n}{n_s}\right)}{\Gamma dt} &= \frac{\frac{n}{s} - 1}{\Gamma T_1} - 4\wp \left| \frac{\sigma}{n_s} \right|^2 \\
 T_1 &= \frac{1}{\gamma_{\uparrow} + \gamma_{\downarrow}}, n_s = \frac{\gamma_{\uparrow} - \gamma_{\downarrow}}{\gamma_{\uparrow} + \gamma_{\downarrow}}, \Gamma = \gamma_p + \frac{1}{2T_1} \\
 \wp &= \wp_0 n_s, \quad \wp_0 = \frac{Ng^2}{\kappa\Gamma}
 \end{aligned} \tag{21}$$

where for threshold parameter, “ $\wp > 1$ ” stimulated oscillations are dominant and for “ $\wp < 1$ ” nanolaser is working in the subthreshold region, and generated plasmons are not coherent. Using this method, quantum fluctuations of plasmon and carrier numbers in the cavity even for a few numbers of plasmons can be estimated. Eventually, you can find first- and second-order correlation functions of the generated plasmons over time for above threshold pumping and the resulting linewidth “ D ” in Eq. (22). Significant linewidth narrowing with respect to the natural broadening “ Γ ” for “ $\wp > 1$ ” implies proper laser operation, and time damping quantum fluctuations can be seen from the second-order correlation function [28].

$$\begin{aligned}
 g_{>}^{(1)}(\tau) &= e^{-(i\omega + D)\tau} \left[1 - DT_1 + DT_1 e^{\frac{\tau}{2T_1}} \cos \left(\frac{\sqrt{2\Gamma T_1(\wp - 1)}\tau}{T_1} \right) \right] \\
 g_{>}^{(2)} &= 1 + 4DT_1 e^{\frac{\tau}{2T_1}} \cos \left(\sqrt{2\Gamma T_1(\wp - 1)} \frac{\tau}{T_1} \right) \\
 D &= \gamma_p \frac{\Gamma T_1}{N} \frac{\wp_0(\wp_0 + 1)}{\wp - 1}
 \end{aligned} \tag{22}$$

3.3 Mean-field atomic-scale model (optical Bloch)

In this model, the classical wave equation is applied to the electric field, while plasmons are assumed quantized, and using Fermi's golden rule, a kinetic equation describing the behavior of plasmons is derived. This model proved to be consistent with the previous model above the threshold while having the advantage to be used for quantum dot gain mediums. Also, Einstein's spontaneous and stimulated emission coefficients can be calculated from this model. Therefore, it can prove the positive effect of increased spontaneous emission due to the Purcell effect on the stimulated emission of the nanolaser. However, similar to the model described in Section 3.2, it needs some simplifying assumptions and works in atomic scales [12].

In this model, the nanoscale system consists of a metal layer with permittivity " $\epsilon(\omega)$ " over a dielectric with permittivity " ϵ_h ." The classic eigenvalue wave equation can be written for the plasmonic eigenmodes according to Eq. (23) [12].

$$\nabla \cdot [\theta(\vec{r}) - s_n] \nabla \phi(\vec{r}) = 0 \quad (23)$$

where " $\theta(r)$ " is equal to "1" inside the dielectric and "0" inside the metal. Corresponding eigenvalues to the n th mode can be derived by Eq. (24) where " Ω_n " is the complex frequency of the n th eigenmode in which the real part is equal to the resonant frequency of n th mode " ω_n " and the imaginary part corresponds to the plasmon decay rate " γ_n " [12].

$$s(\Omega_n) = s_n, \quad s(\omega) \equiv \left[1 - \frac{\epsilon(\omega)}{\epsilon_h} \right]^{-1} \quad (24)$$

Assuming " $\gamma_n \ll \omega_n$ " we can write Eq. (25).

$$\gamma_n = \frac{\text{Im}[s(\omega_n)]}{s'_n}, \quad s'_n \equiv \left. \frac{d \text{Re}[s(\omega_n)]}{d\omega} \right|_{\omega=\omega_n} \quad (25)$$

For the times shorter than the plasmon lifetime " $\tau_n = 1/\gamma_n$," corresponding Hamiltonian to the electric field of the quantized surface plasmons can be expressed by Eq. (26) in which " T " is the integration time and should satisfy " $\tau_n \gg T \gg 1/\omega_n$."

$$H = \frac{1}{4\pi T} \int_{-\infty}^{\infty} \frac{d[\omega \epsilon(\vec{r}, \omega)]}{d\omega} \vec{E}(\vec{r}, \omega) \vec{E}(\vec{r}, -\omega) \frac{d\omega}{2\pi} d^3r \quad (26)$$

Using the extension of the electric field based on the quantized eigenmodes of the system, one can write Eq. (27), and Hamiltonian of Eq. (26) can be written as Eq. (28) which has the standard form of a quantum mechanical harmonic oscillator.

$$\vec{E}(\vec{r}, t) \equiv -\nabla \phi(\vec{r}, t), \quad \phi(\vec{r}, t) = \sum_n \sqrt{\frac{2\pi\hbar s_n}{\epsilon_h s'_n}} \phi_n(\vec{r}) e^{-\gamma_n t} [a_n e^{-i\omega_n t} + a_n^\dagger e^{i\omega_n t}] \quad (27)$$

$$H = \sum_n \hbar \omega_n \left(a_n^\dagger a_n + \frac{1}{2} \right) \quad (28)$$

where “ a ” and “ a^\dagger ” are annihilation and creation operators of plasmons, respectively. Consider dipolar emitters (quantum dots) with carrier population densities of the ground state and excited state equal to “ $\rho_1(r_a)$ ” and “ $\rho_2(r_a)$,” respectively, where “ r_a ” corresponds to the location of the a ’th emitter with transition dipole moment equal to “ d^a .” Transition matrix element [12] for this transition “ d_{10} ” can be estimated by the Kane theory according to Eq. (29) [12] in which “ e ” is the electron charge, “ f ” is the power of the transition oscillator, “ K ” is the Kane constant, “ m ” is the electron mass, and “ ω_n ” is the plasmon frequency of the n th mode. “ d_{10} ” is proportional to the rate of spontaneous emission and Purcell effect.

$$d_{10} = e \sqrt{\frac{fK}{2m_0\omega_n^2}} \quad (29)$$

Interaction between the gain medium and the plasmon modes can be described by Hamiltonian of Eq. (30) which is exerted to the system. Accordingly, using the Fermi’s golden rule, the kinetic equation of the system can be written for the number of plasmons in the n th mode by Eq. (31) in which “ A_n ” and “ B_n ” are the stimulated and spontaneous emission coefficients, respectively [12].

$$H' = \sum_a \vec{d}^{(a)} \cdot \nabla \phi(\vec{r}_a) \quad (30)$$

$$\dot{N}_n = A_n N_n - \gamma_n N_n + B_n \quad (31)$$

According to the mentioned model, Einstein emission coefficients can be derived by Eqs. (32) and (33).

$$A_n = \frac{4\pi s'_n s_n |d_{10}|^2 p_n q_n}{3\hbar \epsilon_h [\text{Im}s(\omega_n)]^2} \gamma_n \quad (32)$$

$$B_n = \frac{4\pi s'_n s_n |d_{10}|^2 r_n q_n}{3\hbar \epsilon_h [\text{Im}s(\omega_n)]^2} \gamma_n \quad (33)$$

where “ p_n ” and “ r_n ” are spatial overlap factors of the n th mode with the gain medium and “ q_n ” is the spectral overlap factor [12]. These parameters can be derived by Eqs. (34–35), respectively.

$$p_n = \int \left[\nabla \varphi_n(\vec{r}) \right]^2 \times \left[\rho_1(\vec{r}) - \rho_0(\vec{r}) \right] d^3r \quad (34)$$

$$r_n = \int \left[\nabla \varphi_n(\vec{r}) \right]^2 \times \rho_1(\vec{r}) d^3r \quad (35)$$

$$q_n = \int F(\omega) \left[1 + \frac{(\omega - \omega_n)^2}{\gamma_n^2} \right]^{-1} d\omega \quad (36)$$

where “ $F(\omega)$ ” is the spectral characteristic of the transition dipole moments.

3.4 Semiclassical rate equations

The aforementioned methods will give us much useful information about the operating principles of the plasmonic nanolasers. However, a consistent model with macroscopic measurable parameters is also needed for larger-scale systems. To do

so, a modified version of an initially proposed rate equation for the microcavity lasers in the 1990s can be used [29, 30]. This model as shown in Eq. (37) according to many recent pieces of research [15, 16, 29] can adequately explain the plasmon/exciton carrier dynamics of a plasmon nanolaser. Furthermore, the macroscopic parameters like output power and pumping current can be easily derived.

$$\begin{aligned}\frac{dn}{dt} &= R_p - An - \beta \Gamma A s (n - n_0) - \frac{nv_s S_a}{V_a} \\ \frac{ds}{dt} &= \beta A n + \beta \Gamma A s (n - n_0) - \gamma s\end{aligned}\quad (37)$$

The first equation of Eq. (6) is expressing the rate of carrier changes, and the second one is describing the temporal behavior of the plasmon generation. Plasmon generation is determined by the spontaneous plasmons coupled in the lasing mode (the first term), stimulated emission (the second term), and plasmon loss rate (the last term) [29].

In these equations “ n ” is the excited state population of the carriers, “ s ” is the number of plasmons in the lasing mode, and “ R_p ” is the carrier generation rate. The coupling factor (β) is defined by the ratio of the spontaneous emission rate into the lasing mode and the spontaneous emission rate into all other modes. A possible calculation method for this parameter can be seen in Eq. (38) [15].

$$\beta = \frac{F_{cav}^{(1)}}{\sum_k F_{cav}^{(k)}} \quad (38)$$

where “ $F_{cav}(k)$ ” is the Purcell factor of k ’th mode. $k = 1$ corresponds to the lasing mode, and the summation is over all of the possible propagation modes in the cavity.

Mode overlap with the gain medium which is also known as Γ -factor is defined by the overlap between the spatial distributions of the gain medium and the lasing mode. In a homogenous medium, spontaneous emission rate “ A ” is equal to “ $1/\tau_{sp0}$ ” and “ τ_{sp0} ” is the spontaneous emission lifetime of the material. However, in a nanocavity, Purcell effect [24] modifies the spontaneous emission rate via “ $A = F_p A_0$,” where “ F_p ” is the Purcell factor and “ A_0 ” is the natural spontaneous emission rate in a homogenous medium. “ n_0 ” is the excited state population of carriers in transparency, “ v_s ” is surface recombination velocity at the sidewalls of the resonator, and “ S_a ” and “ V_a ” are the area of sidewalls of the resonator and volume of the gain medium, respectively. Finally, “ γ ” is the total loss rate of plasmons in the cavity. In order to calculate it, the loss coefficient per unit length should be multiplied by the modal speed. Loss coefficient is calculated by “ $\gamma_m + \gamma_g$ ” where “ γ_m ” and “ γ_i ” are resonator mirror loss and intrinsic cavity loss per unit length, respectively.

4. Different structures of metallic nanoscale plasmon sources

A plasmonic nanolaser needs a metallic nanocavity, gain medium, and a feedback mechanism. In the past two decades, several structures and materials have been introduced for this purpose. Some of these devices are presented in **Figure 4** [13]. These structures can be subwavelength in one dimension like plane nanolaser (see **Figure 5(a)**) [13], in two dimensions like nanowire-based plasmonic nanolaser

(see **Figure 5(b)**) [16], and in three dimensions like nanocavity plasmon laser of [17] (see **Figure 5(c)**).

The gain medium of plasmonic nanolasers can be any material capable of radiative electron decay like any traditional laser. In the proposed structures, a variety of

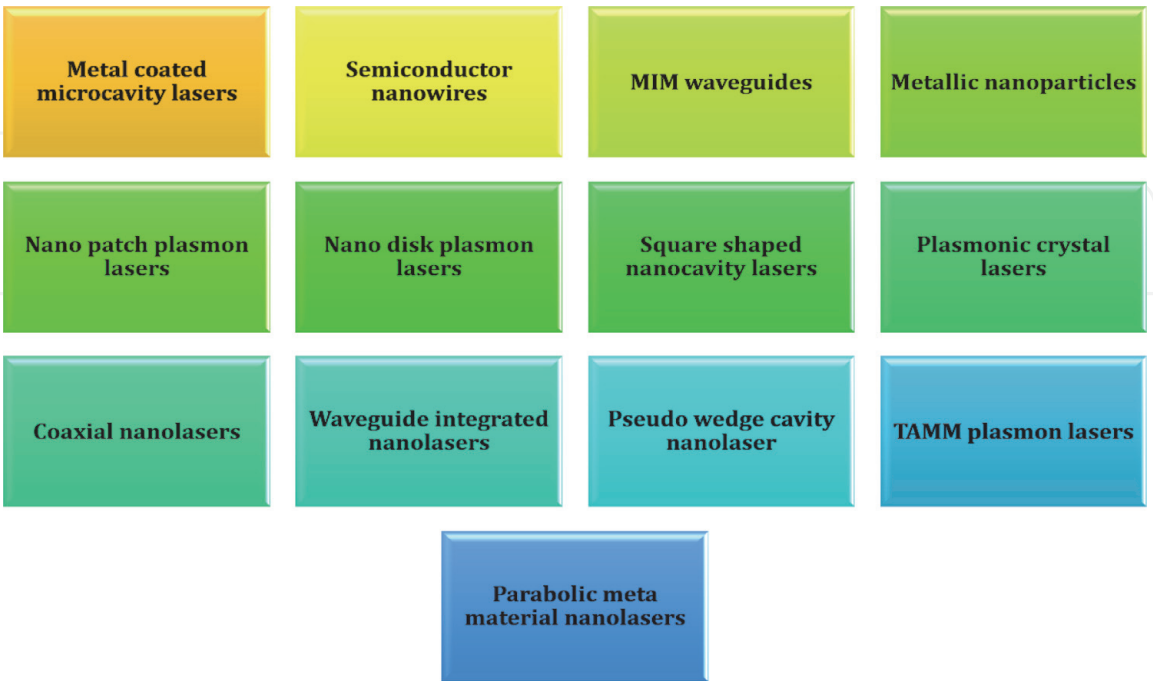


Figure 4.
Different structures of the plasmonic nanolasers [13].

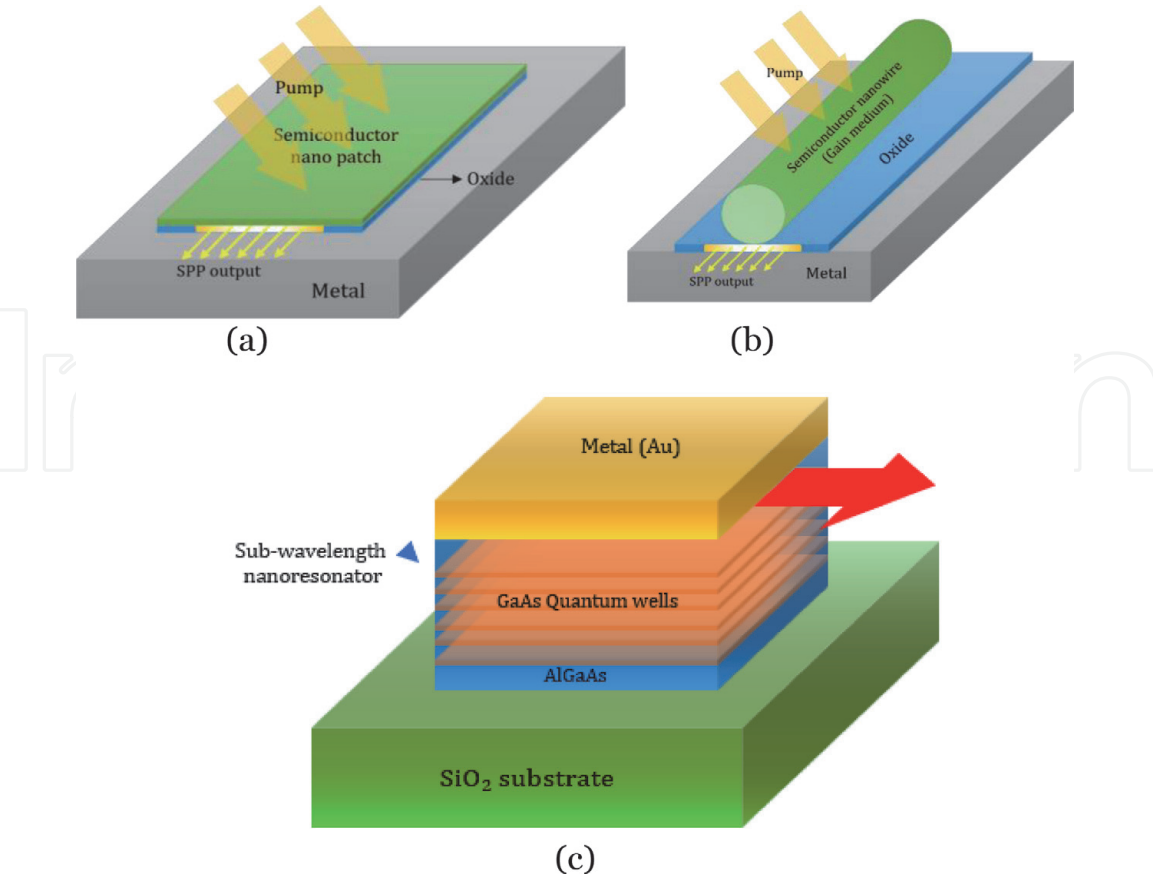


Figure 5.
Different structures of the plasmon nanolasers: (a) a plane plasmon nanolaser [13] (subwavelength in one dimension), (b) typical nanowire-based plasmon nanolaser [16] (subwavelength in two dimension), and (c) quantum well-based nanocavity plasmon laser of [15] (subwavelength in three dimension).

materials like die molecules, bulk semiconductors, semiconductor quantum wells, and quantum dots can be witnessed [13]. Many of the semiconductors were typical optoelectronic materials (III-V and II-IV alloys) like GaAs, AlGaAs, ZnS, InGaAs, InP, and so on [13].

5. Proposed nanoresonator structures

According to our most recent publications [17, 31, 32], we have proposed four nanolaser structures that are discussed in this section. All of these structures are electrically pumped in the room temperature, have subwavelength footprints, and have considerable performance characteristics. The first structure is a GaAs quantum dot-based nanocavity integrated into a plasmonic waveguide [31]. The second is a metal strip nanocavity structure which is based in tensile-strained germanium quantum wells [32]. The next one has a notched nanocavity and germanium quantum wells as the gain medium [17] and the last one is a corrugated metal–semiconductor–metal nanocavity structure utilizing two sets of germanium quantum dot arrays as the gain medium [32].

The first structure is a GaAs/AlGaAs QD nanocavity plasmon laser, which can be integrated into plasmonic waveguides for the realization of integrated plasmonic chips. This proposed nanolaser as sketched in **Figure 6** has several advantages over the previously introduced ones.

For instance, it has a high coupling efficiency to the waveguide plasmonic modes because of its thin structure and the monolithic metal layer. In addition, the proposed nanolaser structure benefits from a large beta factor that means lower threshold and also a high Purcell factor, which leads to higher gain and better laser performance. The MSM structure of this device also can provide an efficient heat transfer performance. Therefore, it predicted to efficiently operate without overheating and needs less chip area for fabrication of heatsink. Nevertheless, the threshold pumping current of the proposed device is considerably high, and this structure cannot provide output power in the mW range in the optimal pumping region. Design characteristics related to the first structure can be seen in **Table 1**.

The second device is a germanium/silicon-germanium (Ge/Si_{0.11}Ge_{0.89}) multiple quantum well plasmonic nanolaser as shown in **Figure 7**. This device utilizes a thin gold metal strip layer, sandwiched between Ge quantum wells in order to maximize both field confinement and exciton-plasmon interaction possibility, which means higher Purcell factor and better gain medium with mode overlap factor. Using two aluminum electrical contacts, one on top of the resonator and one beside it, an electrical pump current can be applied. Moreover, it can be coupled into

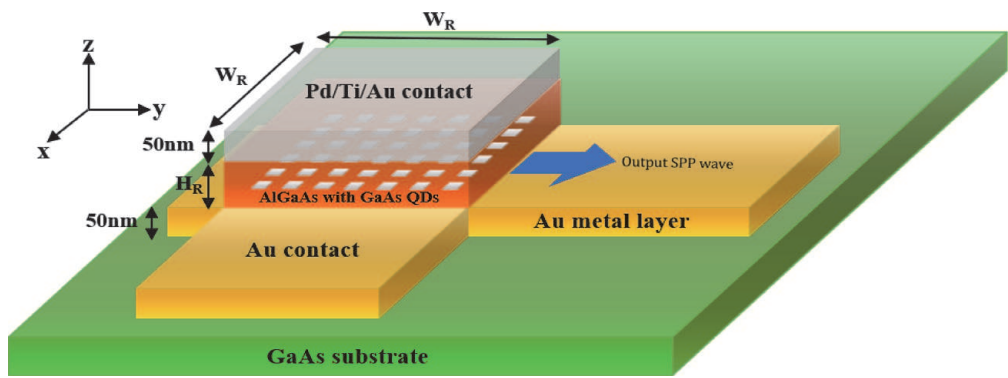


Figure 6.
3D schematic of the GaAs quantum dot-based nanoresonator.

	Symbol	Value
Cavity height	H_R	50 nm
Cavity size	W_R	260 nm
QD size	D_{QD}	5 nm
QD separation	D_{QD2QD}	10 nm
Distance of QDs from gold plate	H_{QD}	25 nm
Top/bottom metal thickness	H_{metal}	50 nm
Doping level (p-type)	N_A	10^{17} cm^{-3}
Doping level (n-type)	N_D	10^{19} cm^{-3}
Number of QDs	N_{QD}	256
QD volume	V_{QD}	$1.25 \times 10^{19} \text{ cm}^{-3}$

Table 1.
Design characteristics of the first structure.

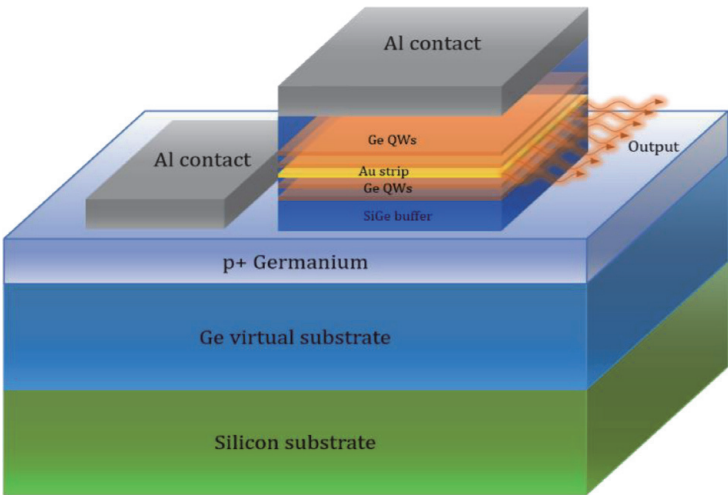


Figure 7.
3D schematic of the metal strip nanocavity structure with germanium quantum wells.

silicon-based waveguides similar to [15] or used in the far-field configuration in which plasmon modes will be converted into photons through the cavity interface. Our device benefits from a metal–semiconductor–metal–semiconductor (MSMS) structure, which can perform well in the 1550 nm regime by means of incorporating highly doped strained Ge quantum wells as the direct bandgap gain medium [33, 34]. Design characteristics of this structure can be found in **Table 2**.

It should be noticed that for transforming germanium into a direct bandgap material, strong tensile strain levels could be applied in the fabrication process. This will reduce the Γ -valley direct bandgap of the material below the L-valley indirect bandgap (0.664 eV) [33, 34]. This will result in an output wavelength about several micrometers in which efficient plasmonic nanocavities cannot be designed. Alternatively, much lower strain level can be utilized, which in combination with extreme level of donor doping for occupying the remaining indirect L-valley states below the Γ -valley results in a direct energy gap diagram [33, 34].

The third structure as shown in **Figure 8** has a cubic nanoresonator with two parabolic notches at both sides. This device provides a high-quality factor and Purcell factor because of the notches which can effectively decrease the output loss (amount of energy escaping the resonator) and improve energy confinement in the cavity. The gain medium of this structure consists of four Germanium quantum

Description	Symbol	Value	Unit
Resonator size	W_R	270	nm
Resonator height	H_R	130	nm
Bottom metal thickness	X_{Strip}	10	nm
Metal thickness	$X_{Contact}$	40	nm
Bottom buffer thickness	X_{Bottom}	15	nm
Top buffer thickness	X_{Top}	15	nm
Number of QWs	N_{QW}	4	—
QW thickness	X_{QW}	7	nm
Barrier wall thickness	$X_{Barrier}$	10	nm
Thickness of p-doped Ge buffer	X_{Buffer}	16	nm
Ge alloy percent	x	89	%
Doping concentration of the QWs and barriers	N_D	7.6×10^{19}	cm^{-3}
Doping concentration of the Ge buffer	N_A	1×10^{19}	cm^{-3}

Table 2.
Design characteristics of the first structure.

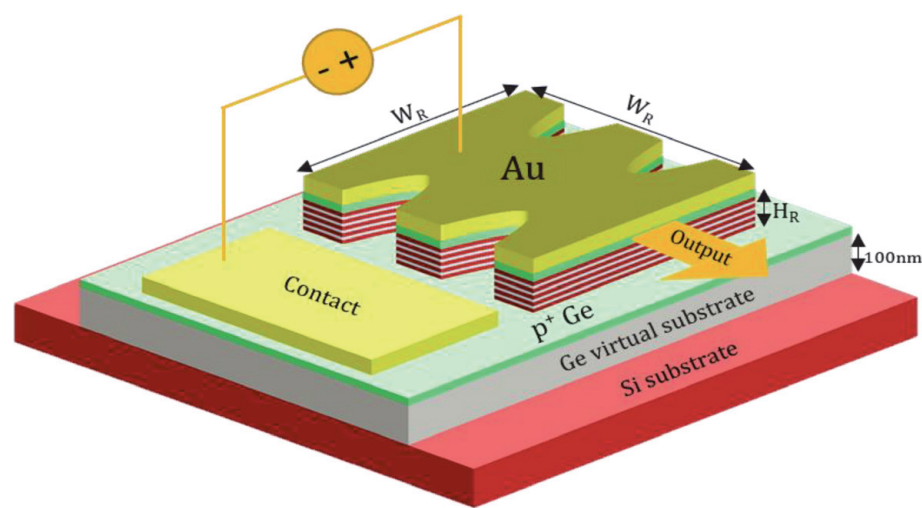


Figure 8.
3D schematic of the notched cavity nanolaser structure.

dots (tensile-strained direct energy bandgap). This structure can be easily integrated into different plasmonic and photonic waveguides with considerable coupling factors. Therefore, it is an appropriate choice for on-chip applications. Also, it can be simply used in the far-field lasing mode. An efficient integration approach can be found in [15]. This device also provides the output free-space wavelength of $1.55 \mu\text{m}$, which means it is compatible with commercial photonic devices and systems. The design characteristics of the third structure can be witnessed in **Table 3**.

The last proposed structure is a corrugated metal-semiconductor-metal nanocavity device that can be seen in **Figure 9**. The specific design of the cavity leads to a significant plasmonic mode with gain medium interaction and also an increase in mode confinement and quality factor. Furthermore, this cavity design using the two-side contacts can provide efficient electrically pumping with a reasonable threshold current. The gain medium of our nanolaser consists of several germanium quantum dots provided on both sides for maximizing the output power.

Description	Symbol	Value	Unit
Resonator size	W_R	350	nm
Resonator height	H_R	98	nm
Top metal thickness	X_{Au}	40	nm
Bottom buffer thickness	X_{Bottom}	10	nm
Bottom buffer thickness	X_{Top}	10	nm
Number of QWs	N_{QW}	4	—
QW thickness	X_{QW}	7	nm
Barrier wall thickness	$X_{Barrier}$	10	nm
Thickness of p-doped Ge buffer	X_{Buffer}	20	nm
Ge alloy percent	x	85	%
Doping concentration of the QWs	N_D	4×10^{19}	cm^{-3}
Doping concentration of the Ge buffer	N_A	1×10^{19}	cm^{-3}

Table 3.
Design parameters of the third structure.

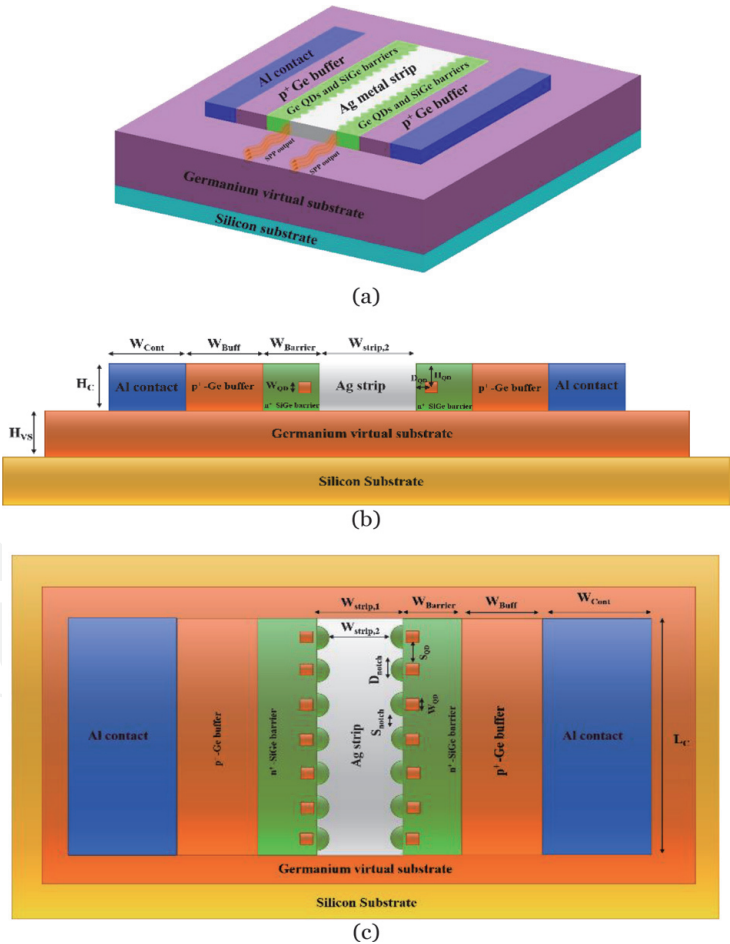


Figure 9.
Schematic illustration of the corrugated lateral MSMSM structure: (a) 3D schematic, (b) transverse cross section, and (c) top view.

The proposed structure for the nanolaser according to **Figure 9** consists of a corrugated metal nanostrip with two arrays of n + doped tensile-strained germanium quantum dots (QDs) at both sides. In addition, two high-doped p + germanium layers are used for better field confinement and providing higher carrier generation

rates in the QDs. This structure also has two aluminum contacts for electrical pumping into the gain medium. In this structure, the electrical pump current flows perpendicular to the plasmonic mode propagation direction into the germanium quantum dots (QDs) in order to produce excitons. This electron–hole pairs

Description	Symbol	Value	Unit
Width of the thick area of the strip	$W_{Strip,1}$	60	nm
Width of the thin area of the strip	$W_{Strip,2}$	50	nm
Height of Ge virtual substrate	H_{VS}	200	nm
Resonator height	H_C	40	nm
Al contact width	W_{Cont}	40	nm
Ge buffer width	W_{Buff}	40	nm
Si-Ge barrier width	$W_{Barrier}$	30	nm
Quantum dot size	W_{QD}	5	nm
Quantum dot distance from the strip	D_{QD}	10	nm
Quantum dot distance from the top	H_{QD}	20	nm
Number of QDs	N_{QD}	34	—
Spacing between QDs	S_{QD}	20	nm
Spacing between two notches	S_{notch}	5	nm
Diameter of notches	D_{notch}	10	nm
Cavity length	L_C	270	nm
Ge alloy percent	x	85	%
Doping level of the QDs and barriers	N_D	4×10^{19}	cm^{-3}
Doping level of the Ge buffer	N_A	1×10^{19}	cm^{-3}

Table 4.
Design characteristics of the lateral MSMSM structure.

Parameter	1st structure	2nd structure	3rd structure	4th structure	Liu et al. [7]
Output wavelength (nm)	850	1550	1550	1550	850
Area (μm^2)	0.07	0.073	0.1125	0.076	0.06
Threshold current (mA)	4.7	29	21	1.9	1.87
Output power in mW at threshold	0.198	4.16	15.6	10.59	0.08
Output power in μW at 10 μA	0.44	2.8	3	50	0.25
Pump current in mA for 1 mW output power	20	~ 7	~ 3	0.2	N.A
Modulation bandwidth in GHz at threshold	3.37	5.7	2.98	28.5	—
Spectral bandwidth in THz at threshold	0.541	1.46	1.98	21.68	>0.08
Purcell factor (lasing mode)	66	291	700	2965	15
Quality factor (Q)	30	26	58	138	32

Table 5.
Performance characteristics of the proposed nanolasers.

recombine through the radiative recombination process and transfer their energy to the surface plasmon polaritons (SPPs) propagating at interfaces of the Ag metal strip and its side semiconductor layers. The design characteristics of this device are provided in **Table 4**.

The introduced nanolaser devices can be adequately analyzed using the aforementioned theoretical phenomena. By means of Finite difference Time Domain (FDTD) method for mode analysis and numerically solving nonlinear rate equations of (37) output performance of the proposed structures can be derived. Also, needed parameters are either extracted from experimental papers or found using numerical methods according to [17, 31, 32]. Resulting from our analysis, the performance of nanolaser structures of 5.1 can be concluded in **Table 5** which demonstrates a considerable performance with respect to a reference similar device [15].

6. Conclusion

In this chapter, we have briefly covered fundamental theories and models related to plasmonic nanolasers. To conclude, nanolasers are one of the most critical building blocks of the future integrated circuits containing both nanophotonics and electronic parts. After two decades of development, recent devices are more promising for the realization of a commercially available nanoscale plasmon source or plasmon nanolaser. Such a device will open a portal to the vast number of potential applications.


Author details

Hamed Ghodsi and Hassan Kaatuzian*

Photonics Research Laboratory (PRL), Electrical Engineering Department,
Amirkabir University of Technology (Tehran Polytechnique), Tehran, Iran

*Address all correspondence to: hsnkato@aut.ac.ir

IntechOpen

© 2020 The Author(s). Licensee IntechOpen. This chapter is distributed under the terms of the Creative Commons Attribution License (<http://creativecommons.org/licenses/by/3.0>), which permits unrestricted use, distribution, and reproduction in any medium, provided the original work is properly cited. 

References

- [1] Einstein A. *Physikalische Zeitschrift*. 1917;**18**:121-128
- [2] Maiman T. Stimulated optical radiation in ruby. *Nature*. 1960; **187**(4736):493-494
- [3] Hall R, Fenner G, Kingsley J, Soltys T, Carlson R. Coherent light emission from GaAs junctions. *Physical Review Letters*. 1962;**9**(9):366-368. DOI: 10.1103/physrevlett.9.366
- [4] Koyama F et al. Room temperature cw operation of GaAs vertical cavity surface emitting laser. *Transactions of IEICE*. 1988;**E71**(11):1089-1090
- [5] Ledentsov N, Ledentsov N, Agustin M, Kropp J, Shchukin V. Application of nanophotonics to the next generation of surface-emitting lasers. *Nano*. 2017;**6**(5):813-829
- [6] Yatsui T. *Nanophotonic Fabrication*. Heidelberg: Springer; 2012
- [7] Taheri AN, Kaatuzian H. Design and simulation of a nanoscale electro-plasmonic 1×2 switch based on asymmetric metal-insulator-metal stub filters. *Applied Optics*. 2014;**53**(28): 6546-6553
- [8] Rastegar Pashaki E, Kaatuzian H, Mallah Livani A, Ghodsi H. Design and investigation of a balanced silicon-based plasmonic internal-photoemission detector. *Applied Physics B*. Dec. 2018; **125**(1)
- [9] Moazzam MK, Kaatuzian H. Design and investigation of a N-type metal/insulator/semiconductor/metal structure 2port electro-plasmonic addressed routing switch. *Applied Optics*. 2015;**54**(20):6199-6207
- [10] Livani AM, Kaatuzian H. Design and simulation of an electrically pumped Schottky-junction-based plasmonic amplifier. *Applied Optics*. 2015;**54**(9):2164-2173
- [11] Enoch S, Bonod N. *Plasmonics*. Heidelberg: Springer; 2012
- [12] Stockman M. The spaser as a nanoscale quantum generator and ultrafast amplifier. *Journal of Optics*. 2010;**12**(2):024004
- [13] Ma R, Oulton R. Applications of nanolasers. *Nature Nanotechnology*. 2018;**14**(1):12-22
- [14] Ginzburg P. Cavity quantum electrodynamics in application to plasmonics and metamaterials. *Reviews in Physics*. 2016;**1**:120-139
- [15] Liu K, Li N, Sadana D, Sorger V. Integrated nanocavity plasmon light sources for on-chip optical interconnects. *ACS Photonics*. 2016; **3**(2):233-242
- [16] Ho J, Tatebayashi J, Sergeant S, Fong C, Ota Y, Iwamoto S, et al. A nanowire-based plasmonic quantum dot laser. *Nano Letters*. 2016;**16**(4): 2845-2850
- [17] Ghodsi H, Kaatuzian H. High purcell factor achievement of notched cavity germanium multiple quantum well plasmon source. *Plasmonics*. 2019. Available from: <https://link.springer.com/article/10.1007%2Fs11468-019-01012-w>
- [18] Yu K, Lakhani A, Wu MC. Subwavelength metal-optic semiconductor nanopatch lasers. *Optics Express*. 2010;**18**:8790-8799
- [19] Kwon SH et al. Subwavelength plasmonic lasing from a semiconductor nanodisk with silver nanopan cavity. *Nano Letters*. 2010;**10**:3679-3683
- [20] Lakhani AM, Kim MK, Lau EK, Wu MC. Plasmonic crystal defect

nanolaser. *Optics Express*. 2011;**19**:18237-18245

[21] Atwater H. The promise of plasmonics. *Scientific American*. 2007; **296**(4):56-62

[22] Kaatuzian H, Taheri A. Applications of Nano-Scale Plasmonic Structures in Design of Stub Filters—A Step Towards Realization of Plasmonic Switches. 2017. [Online]. Available: <http://www.intechopen.com/books/photonic-crystals>

[23] Pitarke JM et al. Theory of surface plasmons and surface-plasmon polaritons. *Reports on Progress in Physics*. 2006;**70**(1):1-87

[24] Francs G et al. Plasmonic Purcell factor and coupling efficiency to surface plasmons. Implications for addressing and controlling optical nanosources. *Journal of Optics*. 2016;**18**(9):094005. DOI: 10.1088/2040-8978/18/9/094005

[25] Nunes FD, Vasconcelos TC, Bezerra M, Weiner J. Electromagnetic energy density in dispersive and dissipative media. *Journal of the Optical Society of America B: Optical Physics*. 2011;**28**:1544-1552

[26] Boriskina S et al. Losses in plasmonics: From mitigating energy dissipation to embracing loss-enabled functionalities. *Advances in Optics and Photonics*. 2017;**9**(4):775. DOI: 10.1364/aop.9.000775

[27] Tame M, McEnery K, Özdemir Ş, Lee J, Maier S, Kim M. Quantum plasmonics. *Nature Physics*. 2013;**9**(6):329-340. DOI: 10.1038/nphys2615 [Accessed: 09 June 2019]

[28] Parfenyev V, Vergeles S. Quantum theory of a spaser-based nanolaser. *Optics Express*. 2014;**22**(11):13671. DOI: 10.1364/oe.22.013671

[29] Ma R, Oulton R, Sorger V, Zhang X. Plasmon lasers: Coherent light source at

molecular scales. *Laser and Photonics Reviews*. 2012;**7**(1):1-21

[30] Yokoyama H, Nishi K, Anan T, Nambu Y, Brorson S, Ippen E, et al. Controlling spontaneous emission and threshold-less laser oscillation with optical microcavities. *Optical and Quantum Electronics*. 1992;**24**(2):S245-S272

[31] Ghodsi H, Kaatuzian H. Design and analysis of an electrically pumped GaAs quantum dot plasmonic nanolaser. *Optik*. 2020;**203**:164027. DOI: 10.1016/j.ijleo.2019.164027

[32] Ghodsi H, Kaatuzian H, Pashaki E. Design and simulation of a Germanium multiple quantum well metal strip nanocavity plasmon laser. *Optical and Quantum Electronics*. 2020;**52**(1). DOI: 10.1007/s11082-019-2172-6

[33] Liu J, Sun X, Pan D, Wang X, Kimerling LC, Koch TL, et al. Tensile-strained, n-type Ge as a gain medium for monolithic laser integration on Si. *Optics Express*. 2007;**15**:11272-11277

[34] Chang G-E, Chen S-W, Cheng HH. Tensile-strained Ge/SiGe quantum-well photodetectors on silicon substrates with extended infrared response. *Optics Express*. 2016;**24**:17562-17571